Journal of Materials Chemistry C

ROYAL SOCIETY OF CHEMISTRY

PAPER

View Article Online
View Journal | View Issue

Cite this: J. Mater. Chem. C, 2023, 11, 5174

Heteroatom-directed supramolecular helical-rich architectures in N-terminal protected pyridyl aromatic amino acids†

Thangavel Vijayakanth, [a] Bin Xue, [c] Sarah Guerin, [d] Sigal Rencus-Lazar, [a] Natalia Fridman, [e] Damien Thompson, [d] Yi Cao [c] and Ehud Gazit *[ab]

Supramolecular helical structures formed by the assembly of biological and bio-inspired building blocks (typically amino acids, peptides and proteins) are an intriguing class of materials with prospective applications in sustainable biomedical technologies and electronics. Specifically, short peptide or single amino acid building blocks can give rise to ideal materials candidates in terms of low cost, adjustability, and compatibility. Yet, to date, reliable helical topologies with specific handedness have been highly challenging to obtain. Herein, we present simple N-terminal protected aromatic pyridyl amino acids that display helicity at the molecular level confirmed by single-crystal X-ray diffraction analysis. The helical structure is stabilized by strong intermolecular hydrogen bonding between the pyridyl nitrogen and carboxylic acid groups. By comparing the specific L and D isomers with the DL racemic mixture, we explicitly demonstrate the influence of amino acid chirality on supramolecular crystal packing, self-assembly, and electromechanical properties. Atomic force microscopy (AFM) nanoindentation analysis confirms the strong rigidity of the DL assembly with very high Young's modulus (31.8 ± 11.9 GPa) attributed to the stacked face-to-face dimers with macrocyclic architectures. The present study provides an effective strategy for precisely formulating supramolecular helical structures, which could pave the way for the development of new bio-electronic applications of smart chiroptical materials from functionalised amino acids.

Received 13th December 2022,
Accepted 7th March 2023

DOI: 10.1039/d2tc05320a

rsc.li/materials-c

Introduction

Chirality is a well-known natural materials property with significant implications from evolutionary biology to sensing technologies.[1–4] A chiral molecule exists in two stereoisomers, termed enantiomers, that are non-superimposable and comprise mirror images of each other, which are often denoted as "D" or "L" forms. Chiral molecules such as L-amino acids and D-sugars are utilized in many biological and bio-inspired systems to execute essential biological functions and control of chirality is essential for crystal engineering, chiroptical, pharmaceutical and biomedical applications.[5–12] Beyond single-molecule chirality based on differences in the single-molecular structure, supramolecular chirality is also observed in materials composed of periodic asymmetric assemblies of molecules (typically, helical and spiral geometry) packed *via* non-covalent interactions. These include electrostatic binding forces, principally hydrogen bonds (H-bonds), and weaker van der Waals forces which are mainly London dispersion forces between transient dipoles.[13–15] Supramolecular secondary structures consist primarily of α-helix and β-sheet motifs. In contrast to the β-sheet, the α-helix conformation is more challenging to obtain, requiring longer amino acid sequences comprising specific residues.[16–20] While proteins typically show right-handed P-helices with rare occurrence of left-handed M-helices, designed supramolecular helical structures are becoming more extensively explored for materials science and technological applications.[21,22] Recently, we have shown that the supramolecular helical structure formed by a minimalistic peptide (Pro-Phe-Phe) confers interesting optical, mechanical and electrical properties.[23,24] With directed

[a] Shmunis School of Biomedicine and Cancer Research, George S. Wise Faculty of Life Sciences, Tel Aviv University, Tel Aviv – 6997801, Israel. E-mail: ehudg@post.tau.ac.il
[b] Department of Materials Science and Engineering, Iby and Aladar Fleischman Faculty of Engineering, Tel Aviv University, Tel Aviv – 6997801, Israel
[c] National Laboratory of Solid-State Microstructure, Department of Physics, Nanjing University, Nanjing 210000, China
[d] Department of Physics, Bernal Institute, University of Limerick, Limerick V94 T9PX, Ireland
[e] Schulich Faculty of Chemistry, Technion-Israel Institute of Technology, Haifa – 32000, Israel

† Electronic supplementary information (ESI) available. CCDC 2211500–2211503. For ESI and crystallographic data in CIF or other electronic format see DOI: https://doi.org/10.1039/d2tc05320a

H-bond interactions between donor and acceptor atoms, other materials have been similarly used to engineer smart crystalline materials.[25–31] However, to date, supramolecular helical structures comprising of ultra-short single amino acids or short (typically, <4) residue peptide sequences have been rarely reported.[32–34]

Here, we addressed the unmet demand for minimalistic supramolecular helical assemblies by developing a strategy based on simple heteroatom-derived aromatic amino acid derivatives. We designed a 9-fluorenylmethoxycarbonyl (Fmoc) protected aromatic pyridyl alanine (PyA) amino acid that self-assembles into a supramolecular helical structure as evidenced by single-crystal X-ray diffraction study. Further, by exploring specific isomers, namely L, D, and DL, we can directly track the hierarchical effect of amino acid molecular chirality on supramolecular crystal packing, self-assembly, and macroscopic mechanical and piezoelectric properties. Moreover, the non-covalent interactions that direct and stabilize the assembly were mapped using digital Hirshfeld 3D-color mapping and 2D-finger print analysis. The DL isomer shows a very high Young's modulus (31.8 ± 11.9 GPa), similar to some metals as well as cortical bones,[35] arising from the constructed strong dimeric macrocyclic H-bonded structures. To the best of our knowledge, this is the first report of supramolecular minimalistic helical structures containing pyridyl nitrogen formed by the use of simple Fmoc-protected aromatic amino acids.

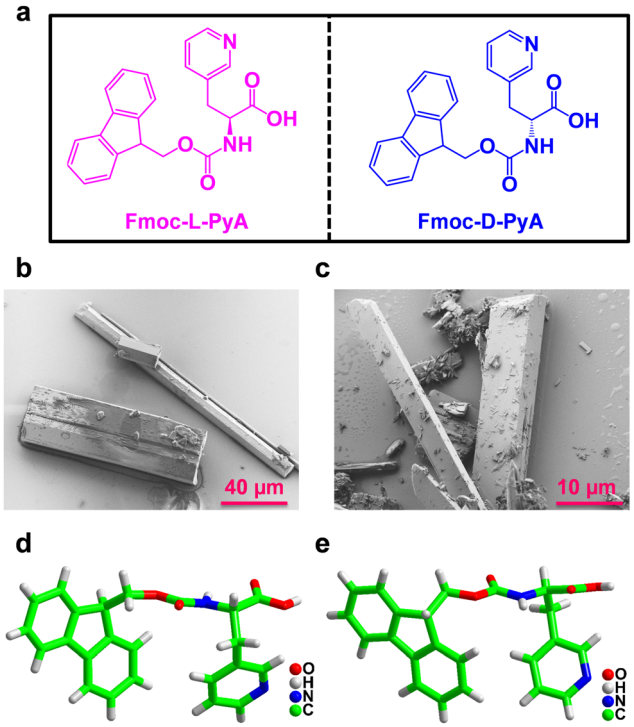

Fig. 1 (a) Molecular structures of enantiopure Fmoc-PyA isomers. (b and c) Scanning electron microscopy (SEM) images of (b) Fmoc-L-PyA and (c) Fmoc-D-PyA crystals. (d and e) Single-crystal structures (asymmetric unit) of (d) Fmoc-L-PyA and (e) Fmoc-D-PyA isomers.

Results and discussions

Structural analysis of Fmoc-PyA

The pure enantiomers Fmoc-L-PyA and Fmoc-D-PyA were crystallized in methanol at room temperature using a slow evaporation technique. For the crystallization of the Fmoc-DL-PyA racemic mixture, a 1 : 1 equivalent of Fmoc-L-PyA and Fmoc-D-PyA isomers was combined in a methanolic solution. Within three days, colourless crystals were formed for all combinations (Fig. 1b and c and Fig. S1–S3, ESI†). Single-crystal X-ray diffraction analysis revealed that Fmoc-L-PyA and Fmoc-D-PyA crystallized in the isostructural non-polar acentric orthorhombic space group $P2_12_12_1$ (Table S1, ESI†). Moreover, Fmoc-DL-PyA crystallized in the centrosymmetric monoclinic space group $P2_1/c$ confirming the racemic mixture of Fmoc-L-PyA and Fmoc-D-PyA isomers. Interestingly, it also produced a variety of polymorphic forms with notable differences in the unit cell parameters. Detailed single crystal data collection and structural refinement parameters obtained for the enantiomers and their conjugate assemblies are summarized in Tables S1–S8 (ESI†).

The asymmetric unit of Fmoc-L-PyA and Fmoc-D-PyA contained one molecule without any co-crystallised solvent (Fig. 1d and e and Fig. S4–S6, ESI†). ORTEP (Oak Ridge Thermal Ellipsoid Plot) analysis showed the ellipsoid thermal behaviour of the enantiomers with similar sizes, shapes and coherent orientations (Fig. S7 and S8, ESI†).

The higher-order packing arrangement revealed intermolecular H-bonded assemblies, including inter-amide and pyridine-carboxylic acid contacts (Fig. 2 and 3a, b). The first formed with a short bond distance of 2.35 Å (N–H···O, bond angle = 144.19°), and the second was mediated by very strong H-bonds in length 1.76 Å (O–H···N, helical bond angle = 167.51°) between the acceptor (pyridyl atom) and the donor (carboxylic acid) motifs (in this case of the L isomer) (Fig. 2a and Fig. S9a and b, ESI†). The observed bond distance is comparable to typical donor-acceptor distances.[36] Moreover, no significant H-bonded networks were observed between the N-terminal amide NH-group and the C-terminal COOH group.

The asymmetric orientation and directional H-bonded molecular organization of these isomers formed the prominent supramolecular helical chiral structures. The L-isomer displayed right-handedness (P-helix) with a helical pitch of ~8.16 Å (Fig. 2b) which is ~1.66 times higher than the known Fmoc-protected phenylalanine (Phe) derivative that shows a typical helical pitch of 4.91 Å (Fig. S10, ESI†) (A helical pitch value of 8.08 Å was observed for the D-isomer, Fig. 2d). Due to the strong interactions of the pyridyl nitrogen with the adjacent carboxylic acid, Fmoc-L-PyA showed a higher helix angle and pitch compared to most known Fmoc-protected amino acids (Fig. 2b and Fig. S10, ESI†).[7,32–34]

It should be highlighted that the fluorene segment displays inverse helicity of M-handedness to that of pyridine-carboxylic acid H-bonded structures for Fmoc-L-PyA in the higher-order

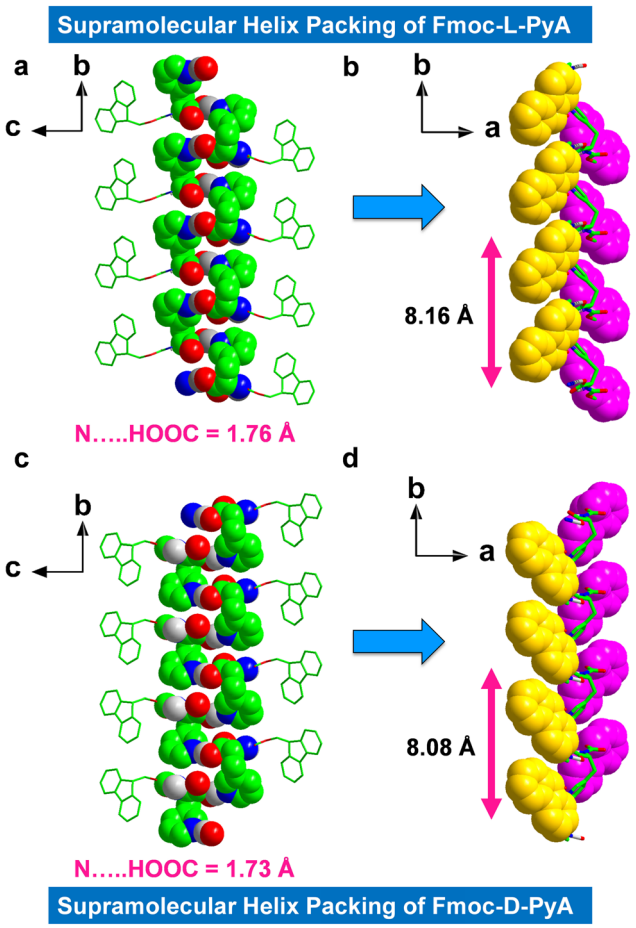

Fig. 2 Crystal packing structures of (a and b) Fmoc-L-PyA and (c and d) Fmoc-D-PyA. The atoms C, H, N and O are coloured green, grey, blue and red, respectively. Panels a and c compare the supramolecular right- and left-handed helical structures mediated by asymmetrical H-bonds between pyridyl nitrogen and carboxylic acid sites on adjacent molecules (front view). The highlighted space-filling mode is shown to visualize the individual chirality of the amino acid residues. Panels b and d highlight the chirality-directed pitch of the tilted aryl group segment (fluorene group, in coloured space-filling representation).

packing topologies (Fig. 2b). As expected, Fmoc-D-PyA showed mirror handedness to Fmoc-L-PyA, assembling in a left-handed M-helix (both pyridine-carboxylic acid and fluorene segment), indicating that amino acid chirality modulates the supramolecular handedness *via* asymmetrical H-bonds (Fig. 2c, d and Fig. S9c, d, ESI†). Such features demonstrate the significance of heteroatom, such as nitrogen, in the emergence of molecular packing, symmetry, and higher-order structures. The aryl groups in both structures showed M-handedness with tilted chirality (Fig. 2b and d). This unexpected lack of mirror-handedness between the fluorene segments of Fmoc-L-PyA and Fmoc-D-PyA suggests that these pyridyl amino acids are distinct from previously-reported Fmoc-protected amino acids.[32–34]

Furthermore, the asymmetric H-bonds between adjacent inter amide sites (typically, N–H and C=O group) were weaker than the rigid helical structures generated between pyridyl-nitrogen and carboxylic acid O–H, resulting in longer H-bond distances of 2.35 Å and 2.19 Å for Fmoc-L-PyA and Fmoc-D-PyA, respectively (O2···H1N1, Fig. 3a and b), with O2···N1 distances of 3.11 Å and 3.06 Å for Fmoc-L-PyA and Fmoc-D-PyA, respectively, comparable to previously-reported distances.[32–34] Moreover, the backbone torsion angles for Fmoc-L-PyA and Fmoc-D-PyA were found to be −157 (Φ), −172 (ψ) and 156 (Φ), 170 (ψ), respectively. Fig. 3a and b displays the spatially induced higher-order structure directed by the asymmetric inter amide H-bonded network highlighting the formation of right and left-handed helix topologies.

To gain further insight into the molecular arrangement of the conjugate assemblies of Fmoc-DL-PyA, the single-crystal structures were analysed in detail (Table S1, ESI†).[37] Unlike the chiral single component crystals, the racemic mixtures were found to crystallize in monoclinic space group $P2_1/c$ validating the formation of a racemic mixture. Interestingly, these racemic mixtures displayed two polymorphic forms [**P1**: a = 25.92 Å, b = 4.93 Å, c = 15.67 Å, volume = 1985 Å^3; **P2**: a = 12.51 Å, b = 30.00 Å, c = 5.78 Å, volume = 2151 Å^3], with iso-structural characteristics of an identical crystal system with the same space group in the crystal lattice (Table S1, ESI†). Fig. 3c shows the **P1** polymorph consisting of a series of discrete strong face-to-face dimers containing macrocycles as indicated by the formation of R_2^2 (18)-type rings. The notation ring (R), which is used to denote the macrocycles formed by intermolecular H-bonds, is frequently used to represent the number of donors (here, 2) and acceptors (2) as well as the overall number of atoms (18) involved in the formation of macrocycles.[38,39] This structure was not apparent in either of the individual chiral crystals. In the higher-order crystal packing diagram of Fmoc-DL-PyA (**P1**), consecutive fluorene segments were separated by a distance of 4.93 Å (Fig. 3c). It should be highlighted that while the **P1** polymorph has been reproduced, multiple attempts to reproduce the **P2** polymorph have been unsuccessful. Although the presence of true polymorphism is thus unknot yet proven, the occurrence of **P2**, likely as a minor state, suggests that individual enantiomers in self-assembled structures are dynamic in nature (Fig. S11, ESI†). Moreover, future characterisation studies using techniques such as thermal analysis, microscopy, solid–solid NMR could lead to a better understanding of the polymorphism in these amino acids.

Circular dichroism (CD) analysis further confirmed the asymmetrical H-bonding packing and handedness of the Fmoc-protected pyridyl amino acids in solution (Fig. S12, ESI†). The CD signal for the Fmoc-L-PyA and Fmoc-D-PyA enantiomers displayed mirrored images of the positive and negative cotton effects, indicating their distinct chirality. The racemic mixture, on the other hand, showed a flat baseline that is optically inactive. Moreover, Fourier-transform infrared (FT-IR) and Raman spectroscopic investigations were employed to examine the structural integrity of the neat enantiomers and the racemic conjugate in solid-state samples (Fig. S13–S18, ESI†). The results showed the major vibrational peaks, notably the O–H stretching (*ca.* 3395 cm^{-1}), N–H stretching (*ca.* 3310 cm^{-1}), and the aromatic vibrational modes of the fluorenyl segment C–H

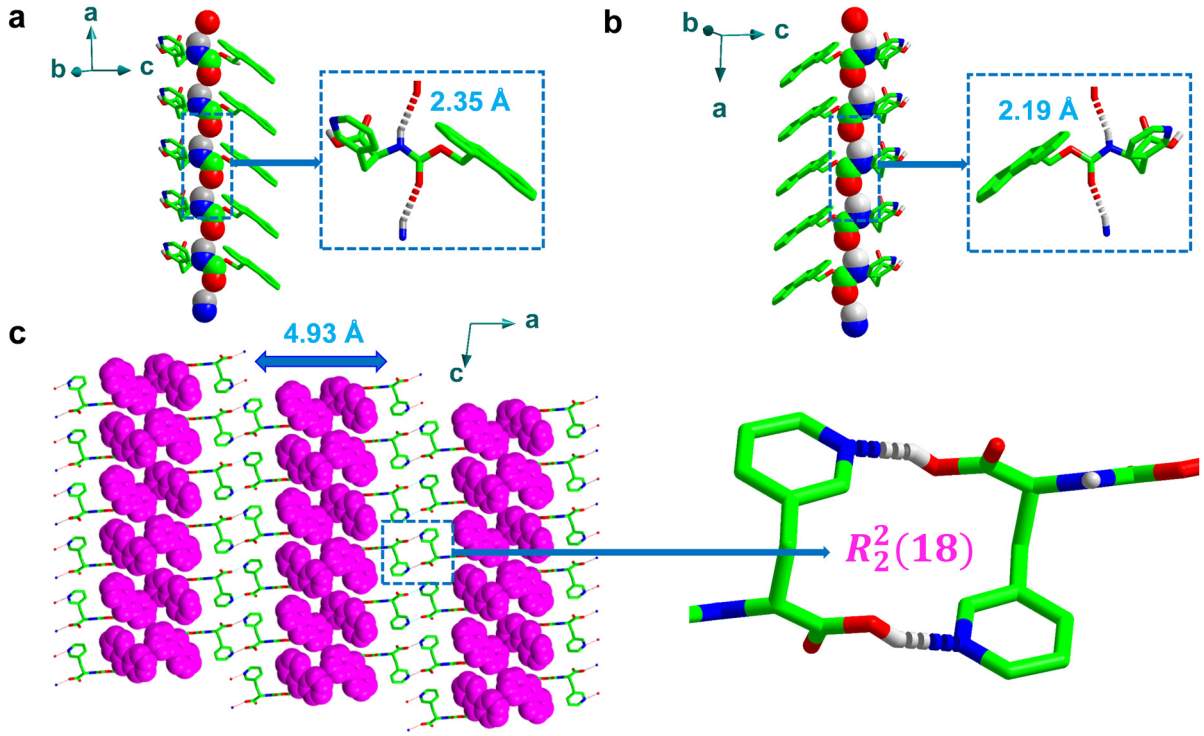

Fig. 3 (a and b) A view of the asymmetrical intermolecular H-bonds formed between amide N–H and C═O groups of (a) Fmoc-L-PyA and (b) Fmoc-D-PyA. (c) Higher-order crystal packing diagram of Fmoc-DL-PyA (**P1**). The space-filling model is shown to visualize the fluorene segment. The dotted square box indicates the H-bonded macrocycle formation with the graph set value of $R_2^2(18)$. The C, H, N, O atoms and the fluorene segment are coloured green, grey, blue, red and magenta, respectively.

bendings (*ca.* 1477 and 1324 cm^{-1}), fingerprinting the pyridyl amino acids (Fig. S13–S15, ESI†). The solution-state absorption spectra of the individual and conjugate assemblies were analysed and the absorption region typically ranged from 250 to 300 nm. Further, the optical bandgap (E_g) was calculated using the Tauc equation $(\alpha h\nu)^2 = A(h\nu - E_g)$, where A is a constant, $h\nu$ is the photon energy, and α is the absorption coefficient. The estimated E_g values ranging from 4.40 to 5.60 eV demonstrate the semiconductive nature of the enantiomers and the conjugate mixtures (Fig. S19–S21, ESI†). Such large bandgap values suggest the potential utilization of these systems in next-generation optoelectronic device applications.[40]

To further investigate the presence of diverse intermolecular interactions (C···H, H···C, N···H, H···N, O···H, H···O, C···C, and H···H), the Crystal Explorer 21.5 software was used to generate three-dimensional (3D) Hirshfeld surface maps and two-dimensional (2D) fingerprint plots based on their single-crystal structures (Fig. S22–S30 and Table S9, ESI†).[41] The Hirshfeld surface was used to quantify and decode the non-covalent interactions using d_{norm} (normalized contact distance), d_e (nearest exterior), and d_i (nearest interior). The 2D and 3D plots of the Fmoc-D-PyA and Fmoc-DL-PyA (**P1**) systems showed very similar intermolecular interaction characteristics (Fig. S25–S30 and Table S9, ESI†). For Fmoc-L-PyA, the strong H-bonding provided $\sim\frac{1}{4}$ of the overall molecular interactions, with a typical stabilizing energy of ~12–30 kJ mol^{-1} per H-bond known to drive the assembly,[42,43] here comprising mainly of pyridyl nitrogen (acceptor)–carboxylic acid (donor) and amino N–H (donor)–amide O═C (acceptor). The remaining interactions stem from dispersion and van der Waals's contacts, individually weak (~0.4–4.0 kJ mol^{-1}) but here covering a large fraction of the intermolecular contact area mainly due to the large fluorene units. Further, we employed powder X-ray diffraction (PXRD) and compared the results with simulated data from single-crystal XRD to validate the bulk phase purity of each individual and racemic mixture form. In comparison to the computer-simulated data, the finely ground powdered crystallites displayed a similar crystalline nature, peak-pattern matching and single-phase identification, confirming the individual structural purity of the samples (Fig. S31–S33, ESI†). In addition to their extensive directional H-bonding arrangement at the molecular level, thermogravimetric analysis (TGA) was used to evaluate the thermal stability of Fmoc-L-PyA, Fmoc-D-PyA, and Fmoc-DL-PyA (**P1**), demonstrating high thermal stability (>500 K) (Fig. S34–S36, ESI†).

Self-assembly studies of Fmoc-PyA

To test for environmental factors, we investigated the self-assembly process of individual chiral and conjugate systems using three different solvent combinations: 100% methanol (MeOH), 90 : 10% MeOH/water (H_2O), and 95 : 5% dimethyl sulfoxide (DMSO)/H_2O while maintaining a constant overall concentration of Fmoc-protected pyridyl amino acids of 1 mg ml^{-1} (Fig. S37–S45, ESI†). Enantiomers and their racemic

mixtures completely dissolved in MeOH and in DMSO. The self-assembled aggregates were visually observed in both the MeOH/H_2O and DMSO/H_2O solvent systems indicating the highly hydrophobic nature of these Fmoc-protected pyridyl amino acids.

The structures self-assembled in pure MeOH formed kinetically-controlled spherical products that varied in length from nano to micrometer scales (Fig. S37–S39, ESI†). Interestingly, the addition of 10% water to produce the MeOH/water mixture transformed the enantiomer spheres into meta-stable ribbon-like structures whereas the racemic assemblies yielded both micro half-spheres and stable self-assembled crystallites (Fig. S40–S42, ESI†). The enantiomers demonstrate the kinetically controlled pathway, but racemic assemblies exhibit both kinetically and thermodynamically controlled by-products. These results indicate the competitive relationship between the kinetic and thermodynamic states of self-assembled products. In addition, for all of L, D, and DL, the H_2O ratio in DMSO determined the self-assembled structure of thermodynamically-stable crystallites (Fig. S43–S45, ESI†). Such diverse self-assembled structures reflect the synergism and cooperativity of diverse weak non-covalent interactions in the self-assembly process, and ease of directing and controlling the solid forms by varying the experimental conditions.[44–48]

Mechanical properties analysis of Fmoc-PyA

Finally, to investigate their potential for utilization as electromechanical device materials, we examined the micromechanical rigidity and stiffness of the crystals using AFM-based nanoindentation experiments (Fig. 4 and Fig. S46, ESI†). The AFM cantilever was positioned to scan the surface of microcrystalline samples spread on a pristine mica substrate and retrieved at a continuous speed of 80 m s^{-1} (Fig. 4a). Further, the Young's modulus was determined using the Hertz model to fit the force-displacement traces (Fig. 4b and Fig. S46, ESI†).

Young's modulus and point stiffness distributions of the enantiomers and racemic mixture are shown in Fig. 4c–h. The measured elasticity of the Fmoc-L-PyA sample showed a Young's modulus of 14.1 ± 4.6 GPa along the elongated direction, indicating lower mechanical stability compared to Fmoc-Phe,[32–34] and a point stiffness value of 281.5 ± 81.5 N m^{-1} (Fig. 4c and d). Fmoc-D-PyA revealed higher Young's modulus and point stiffness values of 23.6 ± 7.1 GPa and 393.1 ± 96.8 N m^{-1}, respectively (Fig. 4e and f). Moreover, Fmoc-DL-PyA (**P1**) displayed a highly increased Young's modulus of 31.8 ± 11.9 GPa, with a point stiffness of 487.8 ± 171.6 N m^{-1}, reflecting the more rigid supramolecular packing network in the racemic crystal (Fig. 4g and h). The order of Young's modulus and point stiffness values is DL > D > L, indicating that the molecular chirality dramatically alters the properties of the crystals. The higher Young's modulus of the DL isomer reflects the formation of the strong discrete dimeric H-bonded structures (Fig. 3c). Remarkably, the measured Young's modulus value is comparable to many well-known bio-inspired and synthetic materials such as collagen, actin, amyloids, bone, wood, silk, Phe–Phe, gold, steel, glass and

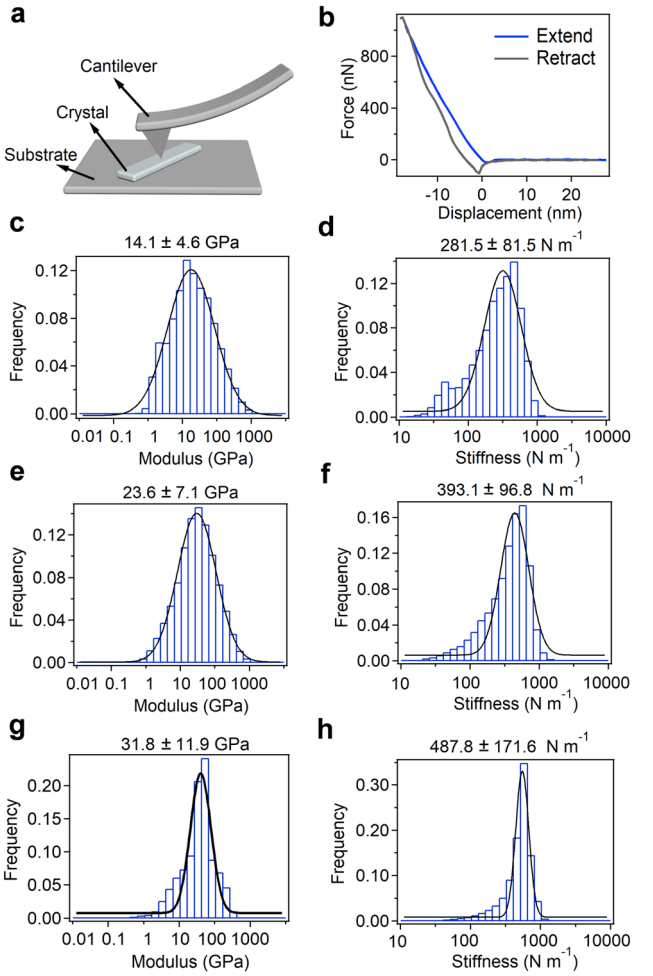

Fig. 4 (a) Schematic diagram of AFM indentation experiments performed on crystal samples. Crystals were deposited on a substrate and the cantilever tip was forced to extend to the crystal sample surface and retract to obtain the force–displacement trace on each spot. (b) Typical force–displacement traces on the peptide crystal. The blue line represents an extension and the grey line represents retraction. (c–h) The statistical Young's modulus (left) and point stiffness (right) distributions of (c and d) Fmoc-L-PyA, (e and f) Fmoc-D-PyA, and (g and h) Fmoc-DL-PyA (**P1**).

metallic alloys,[35,49,50] suggesting their potential use for printed circuit boards (PCBs) and biomedical engineering applications.

Density functional theory simulations of Fmoc-PyA

Bio-inspired materials have emerged as appealing piezoelectric alternatives to conventional inorganic oxides due to their sustainability, easy solution-phase synthesis, biocompatibility, biodegradability, and robust mechanical properties.[51–54] As discussed above, the individual L and D isomers crystallize in non-centrosymmetric orthorhombic space group $P2_12_12_1$. To explore the potential piezoelectric properties, we used density functional theory (DFT) calculations and the obtained magnitude of polarization values are summarized and compared with the well-known supramolecular piezoelectric materials in Tables S10–S12 (ESI†). As expected, crystals of Fmoc-DL-PyA assembled in a centrosymmetric space group, specifically

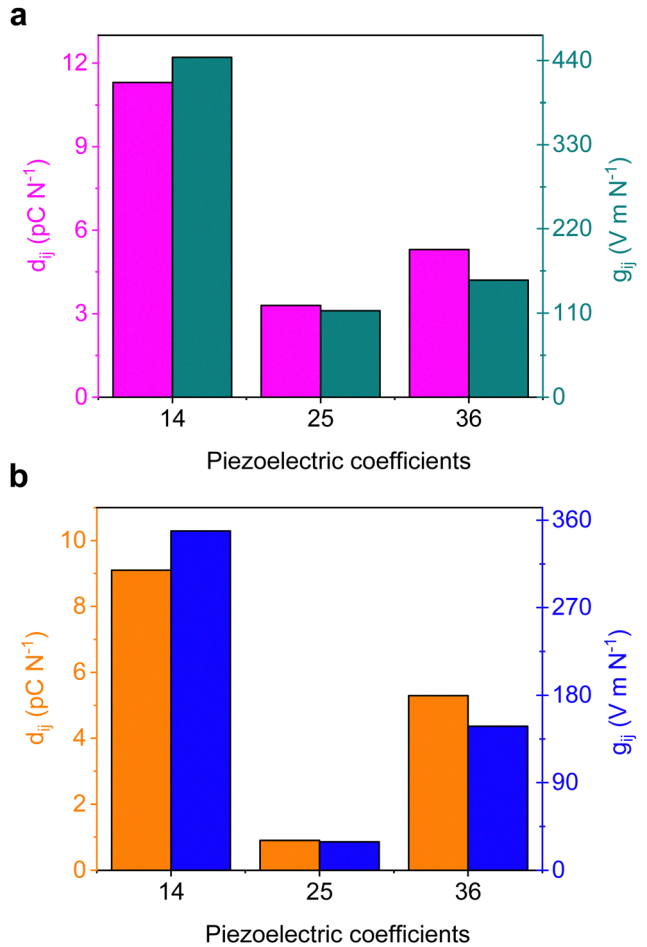

Fig. 5 (a and b) DFT-predicted piezoelectric coefficients of the non-centrosymmetric (a) L- and (b) D-Fmoc-PyA crystal structures.

monoclinic $P2_1/c$, that precludes piezoelectricity. The specific orthorhombic symmetry allows for the presence of three non-zero shear piezoelectric tensor components only: d_{14}, d_{25} and d_{36}. Both enantiopure compounds showed a similar trend in computed piezoelectric response with a maximum predicted strain constant of 11.3 pC N^{-1} in Fmoc-L-PyA (Fig. 5). Additionally, using the relationship between the piezoelectric coefficient (d_{ij}) and the calculated absolute permittivity (ε) of the material ($g_{ij} = d_{ij}/\varepsilon_{ij}$), the piezoelectric voltage coefficient (g_{ij}) characteristics were also predicted. Using the computed relative permittivity of 3.36 and 3.43 for the Fmoc-L-PyA and Fmoc-D-PyA systems, respectively. The maximal g values were g_{14} = 444 and 349 V m N^{-1} for Fmoc-L-PyA and Fmoc-D-PyA, respectively (Fig. 5). Thus, the predicted piezoelectric characteristics reflect the asymmetrical crystal packing of hetero aromatic nitrogen acceptor and carboxylic acid donor atoms of the pyridyl amino acids, which can in the future be utilized to complement inorganic ceramic oxides counterparts, piezo-polymers, and organic and organic–inorganic hybrid materials.[55,56] These characteristics suggest that if a device design allows for the application of shear forces, the enantiopure crystals could display technologically useful energy harvesting capabilities. The significant g_{14} response is oriented along the pyridyl nitrogen–carboxylic acid directed helical structure on the a axis of the crystals (Fig. 2 and Fig. S9, ESI†). Thus, the predicted piezoelectric properties reflect the asymmetrical crystal packing of hetero-aromatic nitrogen acceptor and carboxylic acid donor atoms of the pyridyl amino acids. This type of structure-based design can direct the engineering of new piezoelectric bio-organic and hybrid materials.[55,56]

Conclusions

In summary, we introduce a simple N-terminal protected aromatic pyridyl amino acid that exhibits supramolecular helicity with specific handedness, self-assembled structures, and mechanical and piezoelectric properties. The high-order organization of helicity at the molecular level is revealed by single-crystal X-ray diffraction analysis. The enantiopure form of Fmoc-L-PyA has two helical modalities: amide to amide and pyridine to carboxylic acid (P-helix), and the fluorene groups have distinctive supramolecular tilted chirality (M-helix). Interestingly, the racemic DL mixture was crystallised in two alternative polymorphic forms, demonstrating dynamic interactions between individual enantiomers. Nanoindentation measurements showed that the DL crystal is more mechanically stable than typical biological materials[49,50] due to the rigid structures formed between the donor (carboxylic acid) and acceptor (pyridyl nitrogen atom) sites. Furthermore, DFT calculations predict a significant piezoelectric response in the enantiopure crystals that could be utilized for energy harvesting. This study provides the first demonstration of supramolecular chirality by introducing a heteroatom such as nitrogen into a minimalistic Fmoc-protected aromatic amino acid. The demonstrated effect of chirality in these minimalistic helical assemblies makes them attractive for emerging technologies, such as spin filters for electron transport and enantio-selectors for purification and asymmetric catalysis.[57–60]

Conflicts of interest

There are no conflicts to declare.

Acknowledgements

T. V. thanks Tel Aviv University for the post-doctoral fellowship. E. G. acknowledges the support of the European Research Council PoC project PiezoGel (966813) and Ministry of Science and Technology (MOST) Israel-China Program (3-19130). We thank the members of the Gazit laboratory for helpful discussions. D. T. and S. G. acknowledge Science Foundation Ireland for funding under award number 12/RC/2275_P2 (SSPC) and thank the Irish Center for High-End Computing (ICHEC) for supercomputing resources. S. G. would like to acknowledge funding from Science Foundation Ireland under grant number 21/PATH-S/9737. S. G. is funded by the European Union. Views and opinions expressed are however those of the author only

and do not necessarily reflect those of the European Union or the European Research Council. Neither the European Union nor the granting authority can be held responsible for them.

Notes and references

1 W. Ma, L. Xu, A. F. de Moura, X. Wu, H. Kuang, C. Xu and N. A. Kotov, *Chem. Rev.*, 2017, **117**, 8041–8093.
2 N. A. Kotov, L. M. Liz-Marzán and P. S. Weiss, *ACS Nano*, 2021, **15**, 12457–12460.
3 S. M. Morrow, A. J. Bissette and S. P. Fletcher, *Nat. Nanotechnol.*, 2017, **12**, 410–419.
4 S. Zhang, *Nat. Biotechnol.*, 2003, **21**, 1171–1178.
5 S. F. Mason, *Nature*, 1984, **311**, 19–23.
6 J. Yeom, B. Yeom, H. Chan, K. W. Smith, S. Dominguez Medina, J. H. Bahng, G. Zhao, W. S. Chang, S. J. Chang, A. Chuvilin, D. Melnikau, A. L. Rogach, P. Zhang, S. Link, P. Kral and N. A. Kotov, *Nat. Mater.*, 2015, **14**, 66–72.
7 J. Liang, A. Hao, P. Xing and Y. Zhao, *ACS Nano*, 2021, **15**, 5322–5332.
8 D. Yan, *Chem. – Eur. J.*, 2015, **21**, 4880–4896.
9 M. C. Cringoli, O. Bellotto, R. D. Zorzi, A. V. Vargiu and S. Marchesan, *Synlett*, 2020, 434–438.
10 D. Yan and D. G. Evans, *Mater. Horiz.*, 2014, **1**, 46–57.
11 B. Lu, S. Liu and D. Yan, *Chin. Chem. Lett.*, 2019, **30**, 1908–1922.
12 Y. J. Ma, G. Xiao, X. Fang, T. Chen and D. Yan, *Angew. Chem., Int. Ed.*, 2023, e202217054.
13 P. Xiang and Y. Zhao, *Acc. Chem. Res.*, 2018, **51**, 2324–2334.
14 E. Yashima, N. Ousaka, D. Taura, K. Shimomura, T. Ikai and K. Maeda, *Chem. Rev.*, 2016, **116**, 13752–13990.
15 M. Liu, L. Zhang and T. Wang, *Chem. Rev.*, 2015, **115**, 7304–7397.
16 J. Venkatraman, S. C. Shankaramma and P. Balaram, *Chem. Rev.*, 2001, **101**, 3131–3152.
17 M. Zelzer and R. V. Ulijn, *Chem. Soc. Rev.*, 2010, **39**, 3351–3357.
18 T. E. Creighton, *Nature*, 1987, **326**, 547–548.
19 X. Yan, P. Zhu and J. Li, *Chem. Soc. Rev.*, 2010, **39**, 1877–1890.
20 Z. Luo and S. Zhang, *Chem. Soc. Rev.*, 2012, **41**, 4736–4754.
21 S. Mondal and E. Gazit, *ChemNanoMat*, 2016, **2**, 323–332.
22 W. Ji, B. Xue, S. Bera, S. Guerin, L. J. W. Shimon, Q. Ma, S. A. M. Tofail, D. Thompson, Y. Cao, W. Wang and E. Gazit, *Mater. Today*, 2021, **42**, 29–40.
23 S. Bera, S. Mondal, B. Xue, L. J. W. Shimon, Y. Cao and E. Gazit, *Nat. Mater.*, 2019, **18**, 503–509.
24 S. Bera, S. Guerin, H. Yuan, J. O'Donnell, N. P. Reynolds, O. Maraba, W. Ji, L. J. W. Shimon, P. A. Cazade, S. A. M. Tofail, D. Thompson, R. Yang and E. Gazit, *Nat. Commun.*, 2021, **12**, 2634.
25 O. Dumele, J. Chen, J. V. Passarelli and S. I. Stupp, *Adv. Mater.*, 2020, **32**, 1907247.
26 T. Aida, E. W. Meijer and S. I. Stupp, *Science*, 2012, **335**, 813–817.
27 P. Rozhin, C. Charitidis and S. Marchesan, *Molecules*, 2021, **26**, 4084.
28 K. Ariga, J. Li, J. Fei, Q. Ji and J. P. Hill, *Adv. Mater.*, 2016, **28**, 1251–1286.
29 M. P. Hendricks, K. Sato, L. C. Palmer and S. I. Stupp, *Acc. Chem. Res.*, 2017, **50**, 2440–2448.
30 B. Lu, X. Fang and D. Yan, *ACS Appl. Mater. Interfaces*, 2020, **12**, 31940–31951.
31 S. Li, Y. Lin and D. Yan, *J. Mater. Chem. C*, 2016, **4**, 2527–2534.
32 Z. Zong, A. Hao and P. Xing, *Nanoscale*, 2020, **12**, 20610–20620.
33 Z. Wang, A. Hao and P. Xing, *Chin. Chem. Lett.*, 2021, **32**, 1390–1396.
34 E. R. Draper, K. L. Morris, M. A. Little, J. Raeburn, C. Colquhoun, E. R. Cross, T. O. McDonald, L. C. Serpell and D. J. Adams, *CrystEngComm*, 2015, **17**, 8047–8057.
35 V. Basavalingappa, S. Bera, B. Xue, J. O'Donnell, S. Guerin, P. A. Cazade, H. Yuan, E. U. Haq, C. Silien, K. Tao, L. J. W. Shimon, S. A. M. Tofail, D. Thompson, S. Kolusheva, R. Yang, Y. Cao and E. Gazit, *ACS Nano*, 2020, **14**, 7025–7037.
36 G. J. Jeffrey, *An Introduction to Hydrogen Bonding*, Oxford University Press, New York, 1997.
37 G. M. Sheldrick, SHELXL, *Acta Crystallogr., Sect. C: Struct. Chem.*, 2015, **71**, 3–8.
38 M. C. Etter, *Acc. Chem. Res.*, 1990, **23**, 120–126.
39 G. Bolla, B. Sarma and A. K. Nangia, *Chem. Rev.*, 2022, **122**, 11514–11603.
40 A. Yoshikawa, H. Matsunami and Y. Nanishi, Development and applications of wide bandgap semiconductors, *Wide Bandgap Semiconductors*, Springer, New York, 2007, pp. 1–24.
41 M. J. Turner, J. J. McKinnon, S. K. Wolff, D. J. Grimwood, P. R. Spackman, D. Jayatilaka and M. A. Spackman, *Crystal Explorer 3.1*, The University of Western Australia, 2012.
42 P. Hobza and J. Řezáč, *Chem. Rev.*, 2016, **116**, 4911–4912.
43 K. Müller-Dethlefs and P. Hobza, *Chem. Rev.*, 2000, **100**, 143–167.
44 G. Wei, Z. Su, N. P. Reynolds, P. Arosio, I. W. Hamley, E. Gazit and R. Mezzenga, *Chem. Soc. Rev.*, 2017, **46**, 4661–4708.
45 P. Ke, M. A. Sani, F. Ding, A. Kakinen, I. Javed, F. Separovic, T. P. Davis and R. Mezzenga, *Chem. Soc. Rev.*, 2017, **46**, 6492–6531.
46 J. Wang, K. Liu, R. Xing and X. Yan, *Chem. Soc. Rev.*, 2016, **45**, 5589–5604.
47 S. Gilead and E. Gazit, *Supramol. Chem.*, 2005, **17**, 87–92.
48 G. Wei, W. Xi, R. Nussinov and B. Ma, *Chem. Rev.*, 2016, **116**, 6516–6551.
49 I. Azuri, E. Meirzadeh, D. Ehre, S. R. Cohen, A. M. Rappe, M. Lahav, I. Lubomirsky and L. Kronik, *Angew. Chem., Int. Ed.*, 2015, **54**, 13566–13570.
50 T. P. J. Knowles and M. J. Buehler, *Nat. Nanotechnol.*, 2011, **6**, 469–479.
51 H. Y. Zhang, Z. X. Zhang, X. G. Chen, X. J. Song, Y. Zhang and R. G. Xiong, *J. Am. Chem. Soc.*, 2021, **143**, 1664–1672.

52 T. Vijayakanth, A. K. Srivastava, F. Ram, P. Kulkarni, K. Shanmuganathan, B. Praveenkumar and R. Boomishankar, *Angew. Chem., Int. Ed.*, 2018, **57**, 9054–9058.
53 T. Vijayakanth, F. Ram, B. Praveenkumar, K. Shanmuganathan and R. Boomishankar, *Angew. Chem., Int. Ed.*, 2020, **59**, 10368–10373.
54 Y. M. Wang, Q. Zeng, L. He, P. Yin, Y. Sun, W. Hu and R. Yang, *iScience*, 2021, **24**, 102274.
55 T. Vijayakanth, D. J. Liptrot, E. Gazit, R. Boomishankar and C. R. Bowen, *Adv. Funct. Mater.*, 2022, **32**, 2109492.
56 S. Guerin, A. Stapleton, D. Chovan, R. Mouras, M. Gleeson, C. McKeown, M. R. Noor, C. Silien, F. M. F. Rhen, A. L. Kholkin, N. Liu, T. Soulimane, S. A. M. Tofail and D. Thompson, *Nat. Mater.*, 2017, **17**, 180–186.
57 A. K. Mondal, N. Brown, S. Mishra, P. Makam, D. Wing, S. Gilead, Y. Wiesenfeld, G. Leitus, L. J. W. Shimon, R. Carmieli, D. Ehre, G. Kamieniarz, J. Fransson, O. Hod, L. Kronik, E. Gazit and R. Naaman, *ACS Nano*, 2020, **14**, 16624–16633.
58 W. Mtangi, F. Tassinari, K. Vankayala, A. V. Jentzsch, B. Adelizzi, A. R. A. Palmans, C. Fontanesi, E. W. Meijer and R. Naaman, *J. Am. Chem. Soc.*, 2017, **139**, 2794–2798.
59 L. D. Pachón, I. Yosef, T. Z. Markus, R. Naaman, D. Avnir and G. Rothenberg, *Nat. Chem.*, 2009, **1**, 160–164.
60 K. B. Ghosh, O. B. Dor, F. Tassinari, E. Capua, S. Yochelis, A. Capua, S. H. Yang, S. S. P. Parkin, S. Sarkar, L. Kronik, L. T. Baczewski, R. Naaman and Y. Paltiel, *Science*, 2018, **360**, 1331–1334.